Lasers in Surgery and Medicine 39:118–127 (2007)

Laser Surgery of Port Wine Stains Using Local Vaccum Pressure: Changes in Calculated Energy Deposition (Part II)

Walfre Franco, PhD,[1,2]* Michael Childers, MS,[2] J. Stuart Nelson, MD, PhD,[1] and Guillermo Aguilar, PhD[1,2]
[1]*Beckman Laser Institute, University of California, Irvine, California 92612*
[2]*Department of Mechanical Engineering, University of California, Riverside, California 92521*

Background and Objectives: Application of local vacuum pressure to human skin during laser irradiation results in less absorption in the epidermis and more light delivered to targeted vessels with an increased blood volume. The objective of the present numerical study is to assess the effect of applying local vacuum pressure on the temperatures of the epidermis and small vessels during port wine stain (PWS) laser treatment.
Study Design/ Materials and Methods: Mathematical models of light deposition and heat diffusion are used to compute absorbed energy and temperature distributions of skin and blood vessels with different diameters (10–60 μm) at various depths (200–800 μm) exposed to laser irradiation under atmospheric and vacuum pressures.
Results: Under 50 kPa (15 in Hg) vacuum pressure, peak temperatures at the inner walls of small diameter vessels (10–30 μm) located 200–300 μm below the skin surface are ≈10°C higher than those under atmospheric pressure, and peak temperatures in the epidermis of patients with skin phototype II are ≈5°C lower. In patients with darker skin phototype (IV), the peak temperature at the inner wall of a 10 μm diameter vessel located 200 μm below the skin surface is ≈5°C higher than that under atmospheric pressure, and the peak temperature in the epidermis is ≈10°C lower.
Conclusions: Additional energy deposition in a larger blood volume permits higher temperatures to be achieved at vessel walls in response to laser irradiation. While more energy is deposited in every vessel, temperature gains in small diameter vessels (10–30 μm) are greater, increasing the likelihood of irreversible thermal damage to such vessels. In addition, temperatures in the epidermis decrease because less energy is absorbed therein due to reduced epidermal thickness and concentration of melanin per unit area. Lasers Surg. Med. 39:118–127, 2007. © 2007 Wiley-Liss, Inc.

Key words: PWS; vaccum pressure; energy deposition

INTRODUCTION

The goal of cutaneous laser surgery during treatment of port wine stain (PWS) birthmarks is to cause irreversible thermal damage to vessels while sparing overlying and surrounding tissues [1]. Pulsed dye lasers (PDL) assisted by cryogen spray cooling (CSC) have proven effective for the treatment of PWS [2,3]. However, complete PWS removal is rare even after multiple treatments: most patients obtain a variable amount of PWS blanching and, subsequently, the lesion stabilizes at a red pink color showing little or no improvement despite further laser treatments [4–6]. Clinical studies evaluating the relationship between therapeutic outcome and PWS morphology and anatomic location have found that smaller diameter and deeply located vessels respond poorly to laser treatments: Fiskerstrand et al. [7] reported a PWS vessel mean diameter and depth of approximately 20 and 250 μm, respectively, in patients that responded poorly to PDL; Sivarajan and Mackay [8] reported a reduction in vessel mean diameter from 70 to 40 μm and increased vessel depth from 70 to 85 μm after PDL treatment; the same authors [9] also reported that vessels with diameters of 10–50 μm remained after PDL treatment, while vessels with larger diameters were successfully photocoagulated. Babilas et al. [10] reported incomplete photocoagulation in vessels of 2–16 μm diameter after PDL irradiation of hamster microvasculature.

Although the biological and physical mechanisms of PWS vessel injury remain incompletely understood, a possible mechanism of damage postulates that if the irradiation energy absorbed by hemoglobin is sufficient to increase the vessel wall temperature to 70°C then thermal denaturation occurs [4,8]. In order to confine thermal damage to the vessel, a pulse duration less than the thermal relaxation time (duration for which half of the deposited energy has been lost due to heat diffusion) of the target vessel should be used (usually on the order of milliseconds). It follows that PWS therapeutic outcome relies on the ability of the heated blood volume to increase the vessel lumen temperature to the damage threshold. PWS vessel diameters range from 10 to 100 μm, and from 200 to 1,000 μm in depth [11]; therefore, vessel diameter and depth affect response to laser irradiation. Several studies have shown that specific pulse durations effectively target vessels within a specific diameter range, while smaller and larger vessels require higher fluences (for the same pulse durations) to reach the same average blood temperatures [12–14]. In recent

*Correspondence to: Walfre Franco, PhD, Beckman Laser Institute and Medical Clinic, University of California, 1002 Health Sciences Road East, Irvine, CA 92612.
E-mail: wfranco@uci.edu
Accepted 26 October 2006
Published online 27 February 2007 in Wiley InterScience (www.interscience.wiley.com).
DOI 10.1002/lsm.20464

clinical studies, Svaasand et al. [15] used a pressure cuff on the upper arm of PWS patients to increase the blood volume fraction thereby reducing by 40% the fluence needed to reach the same degree of purpura in the absence of pressure. Aguilar et al. [16] effectively applied local vacuum pressures through suction cups reducing by 35% the fluence needed to reach the same degree of purpura and achieving better PWS blanching as opposed to standard treatment.

OBJECTIVE

The objective of the present numerical study is to assess the effect of mechanical forces induced by local vacuum pressure on the temperature fields of the epidermis and small diameter vessels during PWS laser treatment. To this end, we assess the effect of applying 50 kPa (15 in Hg) vacuum pressure on heat diffusion in the epidermis, dermis, and blood confined in single vessels of constant wall thicknesses, of different diameters, located at various depths. We chose 50 kPa because this is the greatest vacuum pressure that may be applied on human skin without causing discomfort.

NUMERICAL METHODS

The model geometry is illustrated in Figure 1. We use the diffusion approximation to model light deposition; the advantages of using this approximation and a comparison with the Monte Carlo method are presented in the Results section.

Light Deposition

Since light propagation is very fast compared to heat diffusion in biological tissue, light transport is assumed time-independent. The total light fluence rate ϕ_i can be expressed as the sum of the collimated light $\phi_{C,i}$ and diffuse light $\phi_{D,i}$ as

$$\phi_i(x,y) = \phi_{C,i}(x,y) + \phi_{D,i}(x,y), \tag{1}$$

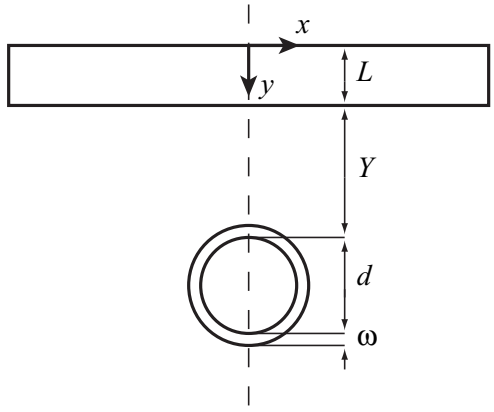

Fig. 1. Model geometry: epidermis, dermis, and single blood vessel. Computational domain: $-500\times10^{-6}\,\text{m} \le x \le 500\times10^{-6}$ m, $0\times10^{-6}\,\text{m} \le y \le 2000\times10^{-6}$ m. $L = 50\times10^{-6}$ m. [Color figure can be viewed in the online issue, which is available at www.interscience.wiley.com.]

where x and y are lateral and depth coordinates, respectively, and the subindex $i = [e,d,w,b]$ denotes epidermis, dermis, vessel wall, or blood, respectively. $\phi_{C,i}$ is defined as

$$\phi_{C,i} = I_{0,i}(y)(1-f_i)\exp(-\mu'_{t,i}y), \tag{2}$$

where $I_{0,i}$ is the flux density at the i surface, f_i is the specular reflectance coefficient and $\mu'_{t,i}$ is the total attenuation coefficient—defined as the sum of the absorption coefficient $\mu_{a,i}$ and the reduced scattering coefficient $\mu'_{s,i}$. $\phi_{D,i}$ is calculated from the steady-state optical diffusion equation

$$\nabla^2\phi_{D,i} - 3\mu_{a,i}\mu'_{t,i}\phi_{D,i} = -\frac{\mu'_{s,i}}{D_i}\phi_{C,i}, \tag{3}$$

where the optical diffusion coefficient $D_i = 1/3\mu'_{t,i}$. Let F_{n+} and F_{n-} be the hemispherical energy fluxes entering and leaving the air–tissue boundary, where a diffuse reflection factor a is introduced to account for scattered light in tissue striking this indexed-mismatched boundary. Applying energy conservation, $F_{n+} = aF_{n-}$. Assuming isotropic radiance and a step function for Fresnel reflection, a is calculated as $1 - r^{-2}$, where the refractive index ratio between tissue and air $r \approx 1.4$, then $a = 0.49$ [17]. At the tissue–air interface (surface boundary condition),

$$\phi_{D,e} = 2AD_e\nabla\phi_{D,e}\cdot\vec{n}, \tag{4}$$

where $\vec{n}$ is the inward unit vector normal to the epidermal surface, and $A = (1+a)/(1-a)$. At other geometry boundaries, $(-500\times10^{-6}, y)$, $(500\times10^{-6}, y)$ and $(x, 200\times10^{-6})$, $\nabla\phi_{D,i}\cdot\vec{n} = 0$.

Heat Diffusion

The heat transfer equation in tissue can be expressed as

$$\rho_i c_i\frac{\partial}{\partial t}T_i(x,y,t) - \nabla(k_i\nabla T_i(x,y,t)) = \mu_{a,i}\phi_i(x,y,t), \tag{5}$$

where ρ_i is the density, c_i is the specific heat, T_i is the temperature, t is the time, and k_i is the thermal conductivity. The term on the right side of Equation 5 accounts for photon absorption by tissue chromophores. In the epidermis, we use a melanosome absorption coefficient of 40,000 1/m at 585 nm [18] and a melanin volume fraction of approximately 7%, which simulates skin phototype II; in the dermis, we use an absorption coefficient corresponding to no blood content; in the vessel wall, we use the same optical properties as the dermis; in blood, we use the absorption coefficient corresponding to an assumed 0.4 hematocrit. The initial ambient temperature of every skin component is 37°C. At the skin surface, the thermal boundary condition is

$$-k\nabla T_e\cdot\vec{n} = h(T_e - T_\infty), \tag{6}$$

where $T_\infty = 37$°C. During and immediately after laser irradiation, air flows over the skin surface, hence a free convection boundary condition is used with the heat transfer coefficient h=150 W/K/m^2 [19]. [At other geometry boundaries, $(-500\times10^{-6}, y)$, $(500\times10^{-6}, y)$,

and $(x, 200 \times 10^{-6})$, $-\nabla T_i \cdot \vec{n} = 0$. Even though the vaporization temperature of blood confined in a vessel is unknown [19], we include the latent heat of vaporization to set an upper bound for temperature gains. The specific heat capacity is modeled as

$$c_i = c_i + v_i \frac{\exp\left(-\frac{(T_i - 110)^2}{\Delta T_i^2}\right)}{\sqrt{\pi \Delta T_i^2}}, \quad (7)$$

where v_i is the latent heat of vaporization and a phase transition is assumed to occur over $\Delta T_i = 1°C$ starting at 110°C. The latent heats of vaporization for epidermis, dermis, vessel wall, and blood are assumed to be 80, 70, 70, and 60% of that of water, $2,250 \times 10^3$ J/kg, based on their water content [21]. It is commonly assumed that blood boils at 100°C because this is the water saturation temperature; however, when heated quickly, a liquid may be superheated well beyond its saturation temperature without a phase change. Hence, the assumed temperature value for the onset of vaporization is somewhat arbitrary.

Optical and thermal properties of epidermis, dermis, vessel wall, and blood at atmospheric conditions are summarized in Table 1, where g is the anisotropy factor used with the Monte Carlo method. The vessel wall is assumed to have negligible effects on light distribution, hence, its optical properties are those of dermis; thermally, it is assumed to have the properties of skin [22].

Effects of Vacuum Pressure

We have investigated the mechanical effects of applying local vacuum pressures on skin using a suction cup—namely, geometrical and optical changes in skin structure [23]. In the present study, we use these results to model vacuum effects as discrete changes with respect to atmospheric conditions; that is, the induced structural changes reach steady state before laser irradiation resulting in new geometry and optical properties related to new skin morphology. The structural changes induced by applying vacuum pressure of 50 kPa to the skin are the following:

- *Reduced epidermal thickness:* Stretching the skin due to suction reduces epidermal thickness; hence, more light is delivered to structures in the dermis. Surface measurements of displacement predict a 10% reduction in epidermal thickness;
- *Reduced concentration of melanin per unit area:* Stretching the skin due to suction alters the spatial distribution of melanin reducing its concentration per unit area; hence, less energy is absorbed in the epidermis and more light is delivered to the dermis. In vivo visual reflectance spectroscopy (VRS) measurements in light and dark skin phototypes show a reduction in epidermal absorption and scattering; results are summarized in Table 2;
- *Displaced blood vessels up toward the surface:* Stretching the skin due to suction forces blood vessels to move up toward the skin surface. Mathematical modeling predicts vertical displacements of 5 μm;
- *Increased blood volume fraction:* Analysis of time-dependent VRS measurements during suction show an overall increase in blood volume fraction from 3 to 11%, Table 2; and,
- *Blood vessel dilation:* Mathematical modeling predicts a 10% increase in blood vessel diameters; however, analysis of VRS measurements shows a potential twofold increase in diameter, Table 3.

RESULTS

The effects of applying 50 kPa (15 in Hg) vacuum pressure, during irradiation with a 1 J/cm^2 0.45 milliseconds 585 nm laser pulse, on heat diffusion in the epidermis, dermis, blood and single vessels of constant wall thickness ($\omega = 5$ μm), different diameters ($d = 10, 20, \ldots, 60$ μm), located at various depths (top of vessel inner-wall, $Y = 200, 300, \ldots, 800$ μm), are evaluated. Finite element analysis (COMSOL, Burlington, MA) is used to solve Equations 1–7. The vessel is assumed to run parallel to the skin surface; thus, solutions are two-dimensional. The modeled changes in geometry and optical properties as a function of pressure are summarized in Table 4.

First, we assess the merits and disadvantages of using the light diffusion approximation. Next, temporal and

TABLE 1. Optical and Thermal Properties [20]. Thermal Diffusivity $\alpha = k/\rho c$

	Property	Epidermis	Dermis	Vessel wall	Blood
Optical	μ_a (1/m)	2,700	24	24	19,100
	μ_s' (1/m)	53,000	12,900	12,900	46,700
	g	0.79	0.79	0.79	0.995
	r_r	1.37	1.37	1.37	1.33
Thermal	c (J/kg K)	3,600	3,800	3,700	3,600
	v (J/kg K)	$1,800 \times 10^3$	$1,575 \times 10^3$	$1,575 \times 10^3$	$1,350 \times 10^3$
	ρ (kg/m^3)	1,200	1,200	1,200	1,057
	k (W/m K)	0.21	0.53	0.41	0.55
	α (m^2/second)	0.5×10^{-7}	1.2×10^{-7}	0.9×10^{-7}	1.5×10^{-7}

TABLE 2. Epidermal Absorption, Epidermal Scattering, Dermal Scattering, and Blood Volume Fraction for Two Different Pressures in Skin Types II/IV [23] at 585 nm

	$\mu_{a,e}$ (1/m)	$\mu'_{s,e}$ (1/m)	$\mu'_{s,d}$ (1/m)	BVF (%)
P_a	2,700/10,400	53,000/60,000	14,800/17,800	3/3
$P_v = 50$ kPa	1,900/6,800	46,000/54,200	15,000/19,600	11/10

spatial profiles of temperature as a function of vessel diameter are shown to illustrate the effect of vessel dilation only on the temperature field. Finally, the effect of mechanical deformation on the temperature field due to vacuum pressure is presented.

Modeling of Energy Deposition

Figure 2 shows the volumetric heat source due to light deposition, Q_L, as a function of depth computed with the diffusion approximation and the Monte Carlo method MAGNUM—developed by Pfefer et al. [24]—for a flux density of 2,000 W/cm^2 and optical properties in Table 1, except $\mu_{a,e} = 1,800$ 1/m and $\mu'_{s,e} = 47,000$ 1/m. Cubic voxels of 1 μm in a $500 \times 2,000$ μm computational domain and 30×10^6 photons are used in the Monte Carlo calculations, which are, computationally, very expensive simulations. Figure 2a shows Q_L along the vertical axis of symmetry across the epidermis, dermis and a 20 μm diameter blood vessel at 250 μm depth. Figure 2b shows Q_L for a 60 μm diameter blood vessel at the same depth. As expected, diffusion theory overestimates energy deposition quantitatively, especially in the epidermis and blood where light absorption is significant; that is, where light propagation is not dominated by scattering. Qualitatively, the difference in energy distribution increases as blood vessel diameter increases, especially within the lower half of the vessel. In spite of these quantitative and qualitative differences, we use the diffusion approximation because of flexibility for finite element implementation and speed in computations.

According to [13], less than 1 J/cm^2 is required to rise the average temperature of vessels of 20, 30, 40, 50, and 60 μm diameter (and 250 μm depth) to 70°C using a 0.45 milliseconds 585 nm laser pulse, while a vessel of 10 μm diameter requires more than 1 J/cm^2 to reach the same average temperature. These are results from computations with the Monte Carlo method. Using the diffusion approximation, the average temperatures for the same vessel diameters (10, 20, 30, 40, 50, and 60 μm, and 200 μm depth) and 1 J/cm^2 laser fluence are 63, 81, 84, 80, 74, and 70°C. These results are comparable to the Monte Carlo computations. As shown, significant differences are expected to occur as the vessel size increases, particularly in temperature distributions within the blood vessel.

TABLE 3. Epidermal Absorption, Vessel Diameter, and Epidermal Reduction Factor as a Function of Vacuum Pressure From VRS Measurements

P_v (kPa)	0	17	34	51
$\mu_{a,e}$ (1/m)	2,700	2,400	2,100	1,900
d (μm)	10	19	20	23
F_e (%)	0	4	8	12

Temporal and Spatial Temperature Profiles

Figure 3 shows the evolution in time of temperature at the vessel center, T_b^c, and the top of the vessel inner-wall, T_w^t, for vessels of 10, 20, and 60 μm diameter located at $Y = 200$ μm. As expected, the time-evolution of temperature during heating and cooling of blood and vessel is diameter–dependent. Figure 3a illustrates that as diameter increases, time-evolution of temperature at the vessel center changes from second-order to linear during heating; and, during cooling (when laser irradiation stops) it changes from exponential decay to increase of temperature (even after irradiation is complete) and slow decay thereafter; temperature increase at the vessel center after irradiation is due to heat diffusion from the blood vessel periphery. Figure 3b illustrates that the time-evolution of temperature during heating at the vessel wall is qualitatively similar to that at the center, and that it follows an exponential decay during cooling. During laser irradiation of small vessels, high amounts of energy per unit volume are instantaneously, uniformly deposited in blood; hence, large heat fluxes are established from blood to the surrounding tissue—energy is dissipated too quickly from the vessel to increase the wall temperature to the damage threshold. In large vessels, lower energy is instantaneously, nonuniformly deposited in blood; hence, smaller heat fluxes are established from the periphery of the blood to the center of the vessel and, also, to the surrounding tissue—energy is poorly distributed and not sufficient to increase the wall temperature to the damage threshold.

Depth profiles of temperature along the axis of symmetry at selected times during laser irradiation ($t = 0–0.45$ milliseconds every 0.05 milliseconds) are shown in Figure 4; the uppermost curve in each figure corresponds to the end of the laser pulse. As vessel diameter increases, temperature profiles go from a single T peak at the vessel center, Figure 4a–d, to two T peaks and one valley, Figure 4e–f. Figure 4f shows that T_b^c for a 60 μm diameter vessel in Figure 3a does not represent the highest blood temperature, and that T_b^c increases after laser exposure because heat diffuses away from the blood vessel periphery at higher T_b. Figure 4a–f shows that there is a vessel diameter for which T_b is the highest overall; that is, specific laser

TABLE 4. Geometry and Optical Properties at Atmospheric and Vacuum Pressures

	L_e (m)	$\mu_{a,e}$ (1/m)	$\mu'_{s,e}$ (1/m)	Y (μm)	d
P_a	50×10^{-6}	2,700	53,000	Y	d
$P_v = 50$ kPa	45×10^{-6}	1,900	46,000	Y-5	d+0.1d

parameters are optimal for a specific vessel diameter. Figure 4a–f also shows that temporal and spatial changes in heat transfer in the epidermis are independent of changes in a single vessel during short periods of time.

Effect of Vacuum Pressure on Temperature Field

Figure 5 shows temperatures at the vessel center and at the top of the vessel inner-wall at the end of the laser pulse at atmospheric pressure, as a function of vessel diameter for different depths. In Figure 5a the vessel that reaches the highest T_b^c has a 30 μm diameter. As vessel depth increases, the differences in T_b^c between vessels of different diameters decrease. In Figure 5b, the vessels that reach the highest T_w have 20 and 30 μm diameters. As vessel depth increases, there are no significant differences in T_w between vessels of

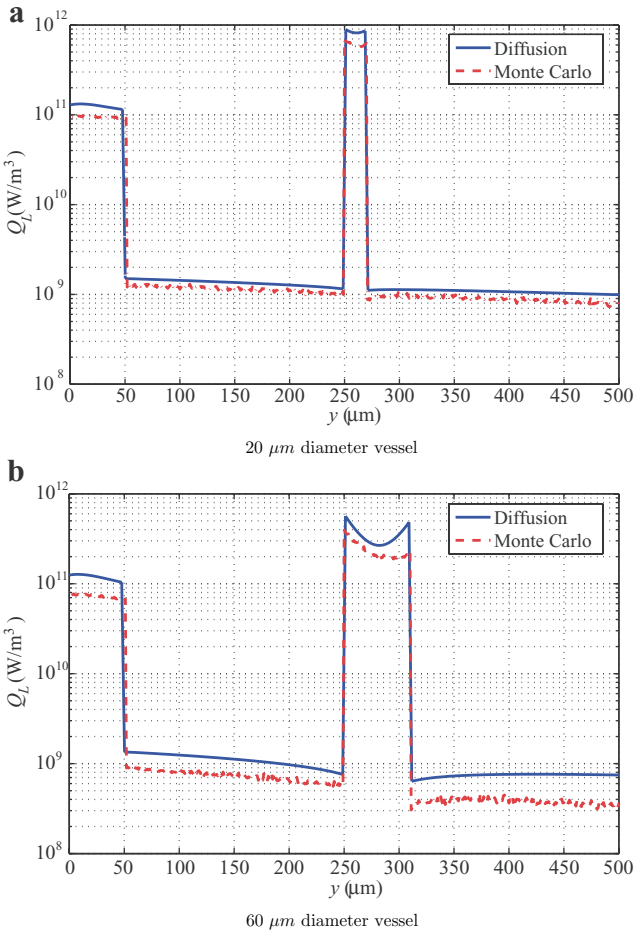

Fig. 2. Depth distribution of power per unit volume due to light deposition for (**a**) 20 and (**b**) 60 μm vessel diameters. $I_0 = 2{,}000$ W/cm^2, $Y = 250$ μm. [Color figure can be viewed in the online issue, which is available at www.interscience.wiley.com.]

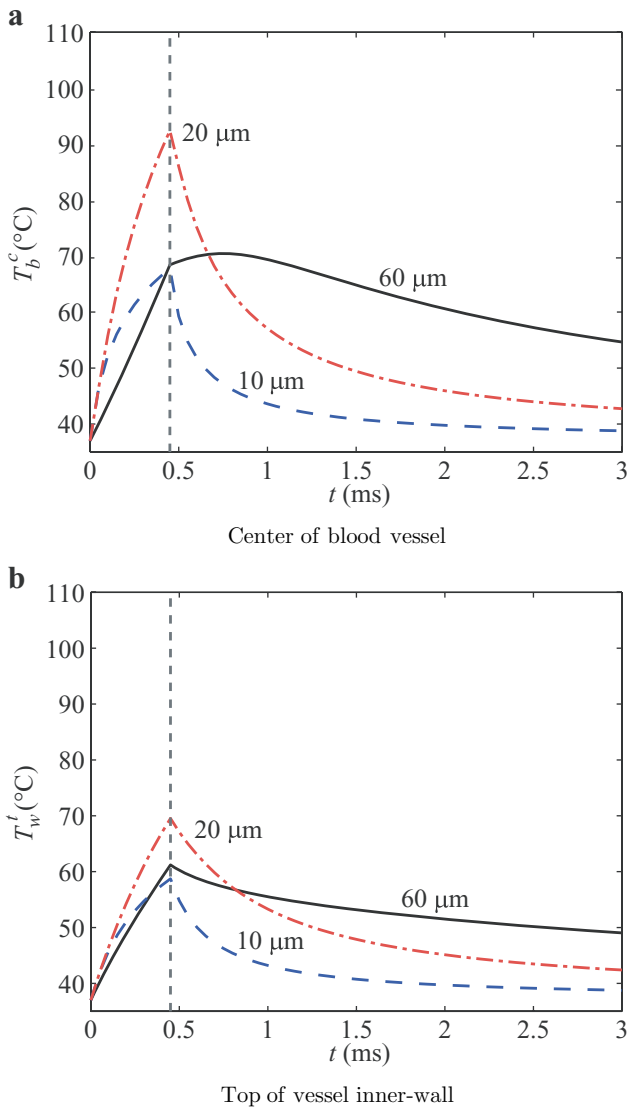

Fig. 3. (**a**) Blood and (**b**) wall temperature as a function of time for vessels of different diameters at atmospheric conditions; vertical line denotes the end of 1 J/cm^2, 0.45 milliseconds laser pulse. $Y = 250$ μm. Skin phototype II. [Color figure can be viewed in the online issue, which is available at www.interscience.wiley.com.]

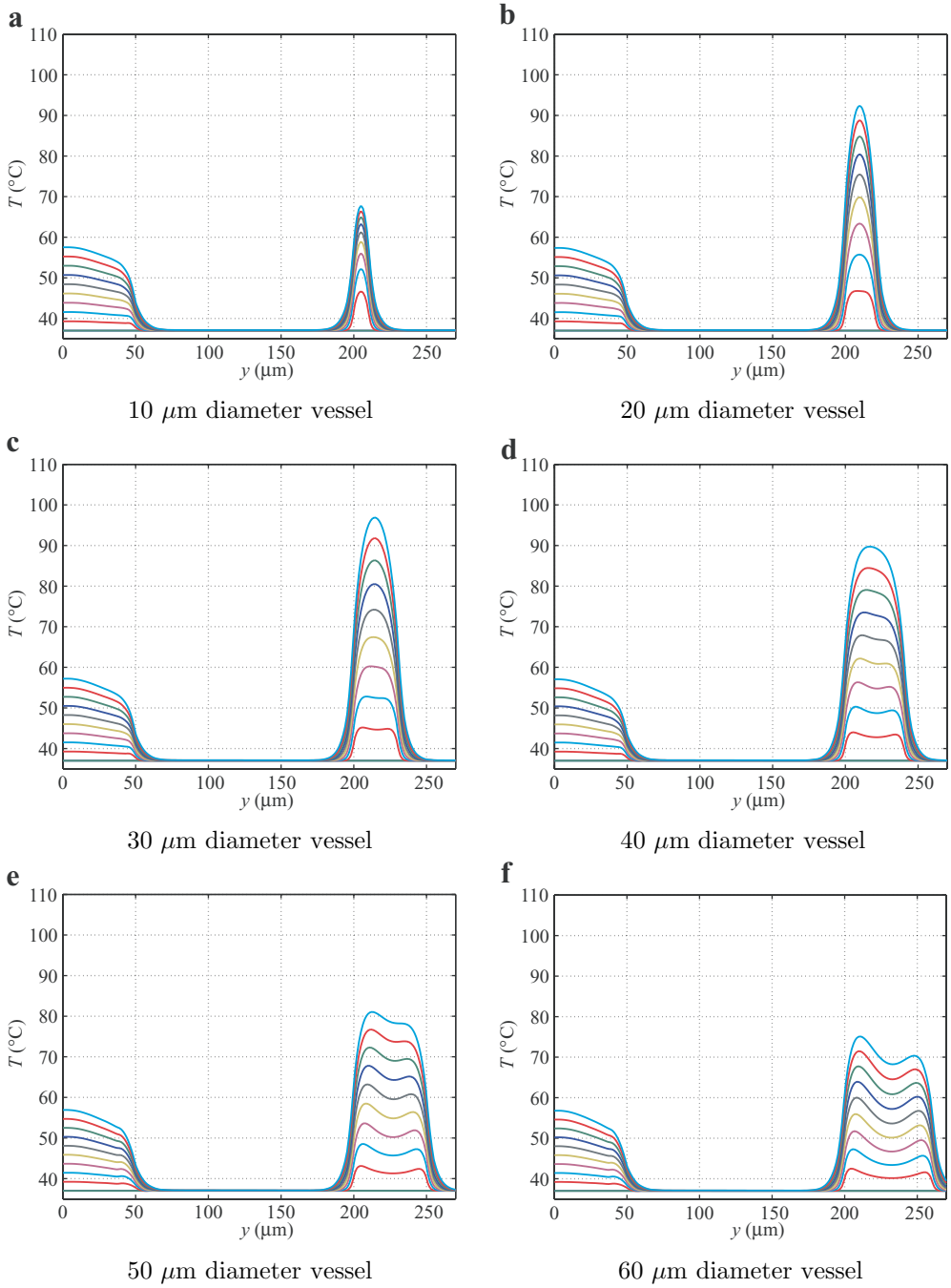

Fig. 4. Depth profiles of temperature during laser irradiation of vessels of (**a**) 10, (**b**) 20, (**c**) 30, (**d**) 40, (**e**) 50 and (**f**) 60 μm diameter at atmospheric conditions; each curve correspond to a specific time, $t = 0, \ldots,$ 0.45 milliseconds in 5 milliseconds increments. 1 J/cm^2, 0.45 milliseconds laser pulse. Skin phototype II. [Color figure can be viewed in the online issue, which is available at www.interscience.wiley.com.]

different diameters. It follows that (smaller and larger) vessels outside of a specific diameter range may not be sufficiently heated for irreversible thermal damage.

Depth profiles of temperature at the end of the laser pulse are shown in Figure 6 for vessels of 10 and 60 μm diameters under atmospheric and vacuum pressures. Figure 6a also shows results of modeling skin phototype IV using the optical properties in Table 2. (Except for this figure, skin phototype II is modeled elsewhere). In addition to the effects of vacuum on tissue optical structure, the

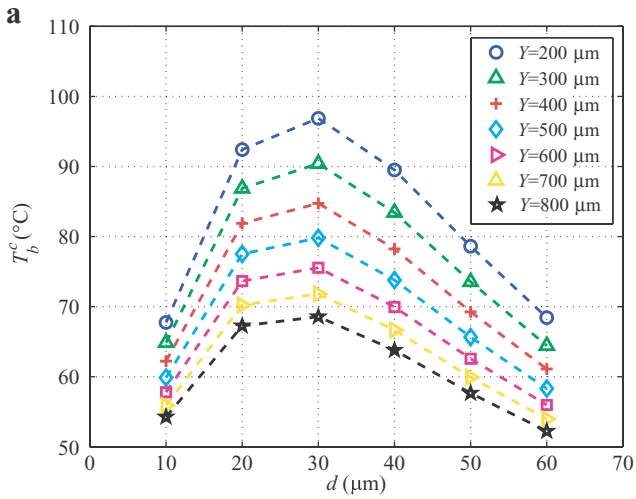

Center of blood vessel

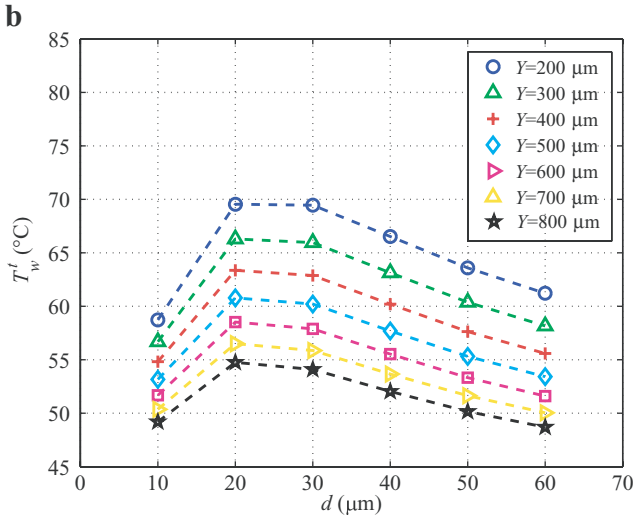

Top of vessel interior-wall

Fig. 5. (**a**) Blood and (**b**) wall temperatures at the end of the laser pulse as a function of vessel diameter for different vessel depths Y. Atmospheric pressure. 1 J/cm^2, 0.45 milliseconds laser pulse. Skin phototype II. [Color figure can be viewed in the online issue, which is available at www.interscience.wiley.com.]

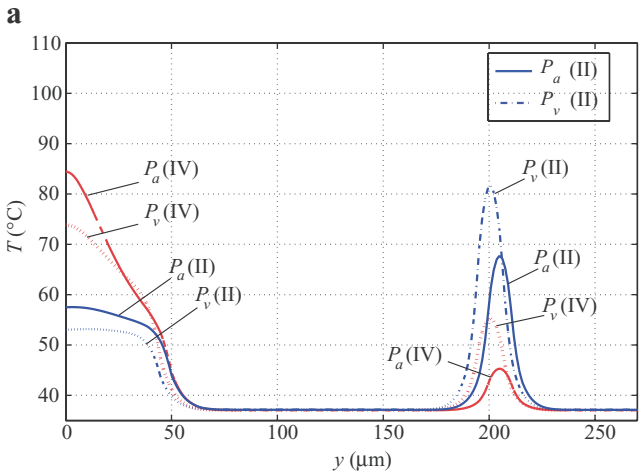

10 μm vessel diameter, skin phototypes II and IV

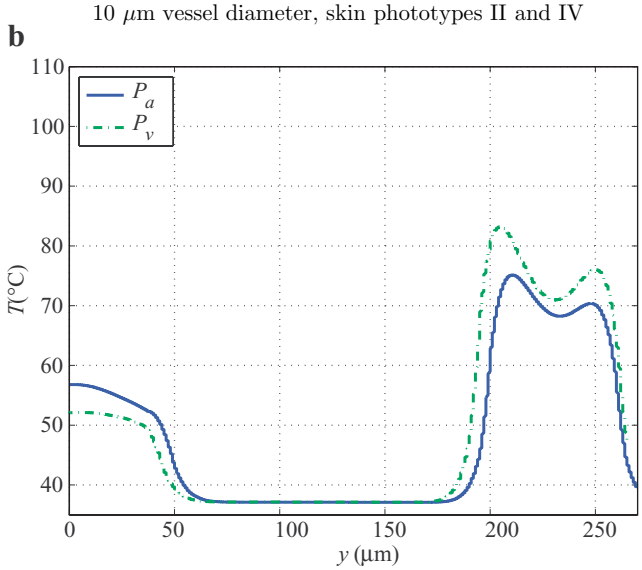

60 μm vessel diameter, skin phototype II

Fig. 6. Comparison of temperature profiles at the end of laser exposure between atmospheric and vacuum (50 kPa) pressures. 1 J/cm^2, 0.45 milliseconds laser pulse. $Y = 200$ μm. (**a**) 10 μm vessel diameter. (**b**) 60 μm vessel diameter. [Color figure can be viewed in the online issue, which is available at www.interscience.wiley.com.]

temperature profiles show the effects on tissue morphology: reduction in epidermal thickness, displacement of vessels up toward the skin surface, and increase in vessel diameter (i.e., increased blood volume).

ΔT is defined as the difference in temperatures between vacuum and atmospheric pressures. ΔT_b^c and ΔT_w^t as functions of vessel diameter and depth are presented in Figure 7. In Figure 7a, ΔT_b^c for $Y = 200$ μm and $d = 20$ and 30 μm are smaller or equal to those of the same d but at deeper locations ($Y = 300$ and 400 μm) because T_b^c at vacuum pressure has reached 110°C, which is the assumed temperature for a phase change. These results assume a 10% vessel dilation calculated from a mathematical model [23].

Figure 8 shows changes in the temperature profiles of a 10 μm diameter vessel as a function of vacuum pressure using the vessel dilations and reduced epidermal thicknesses calculated from in vivo VRS measurements. Table 3 shows $\mu_{a,e}$, d, and F_e (factor of epidermal reduction) as a function of vacuum pressure.

DISCUSSION

The purpose of applying local, controlled, external vacuum pressures to PWS skin is to dilate small resilient blood vessels, such that heat losses during and after laser irradiation are reduced, enhancing irreversible thermal damage to the vessel wall. Svaasand et al. [15] induced temporal dilation of vessels by blocking venous return with

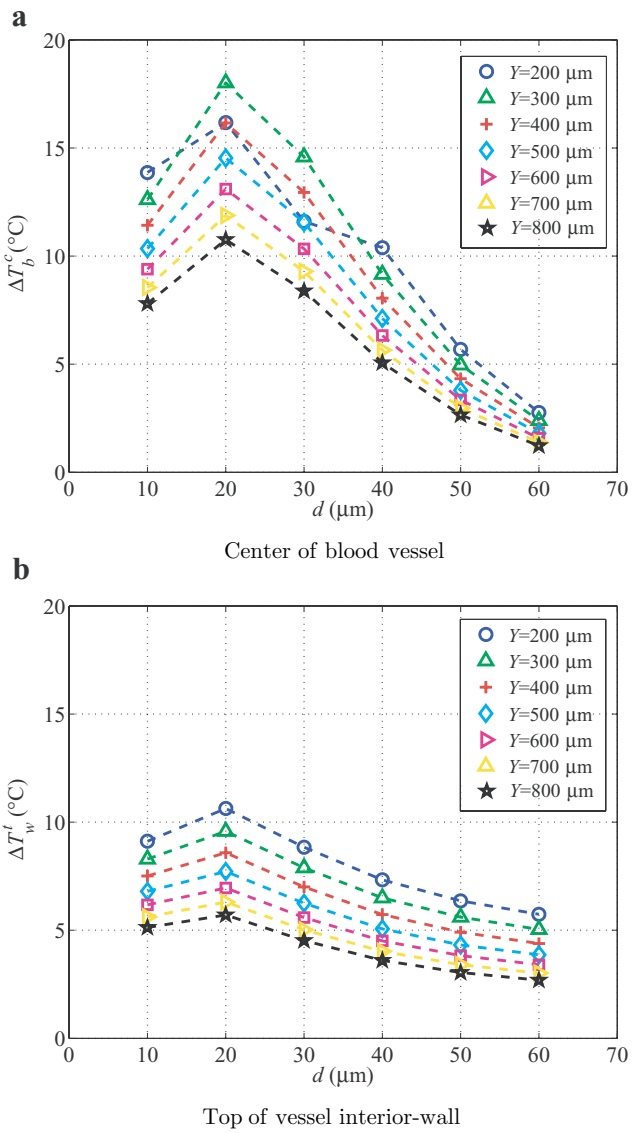

Fig. 7. Differences in (**a**) blood and (**b**) wall temperature at the end of laser exposure between vacuum (50 kPa) and atmospheric pressures as a function of vessel diameter for different vessel depths Y. 1 J/cm^2, 0.45 milliseconds laser pulse. Skin phototype II. [Color figure can be viewed in the online issue, which is available at www.interscience.wiley.com.]

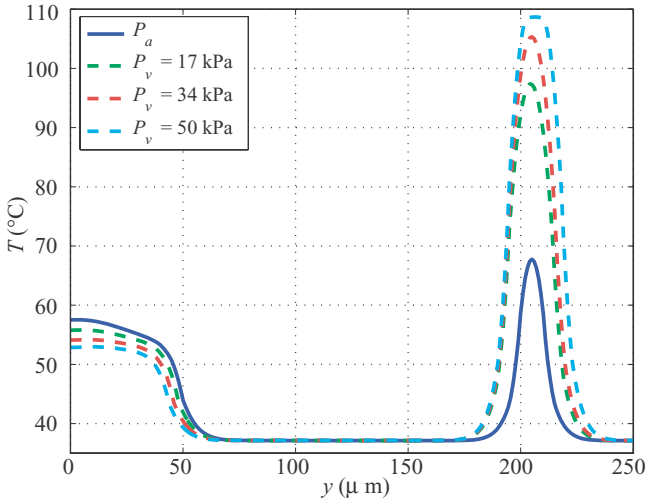

Fig. 8. Comparison of temperature profiles at the end of laser exposure between atmospheric and different vacuum pressures; $d = 10$ μm, $Y = 200$ μm. 1 J/cm^2, 0.45 milliseconds laser pulse. Skin phototype II. [Color figure can be viewed in the online issue, which is available at www.interscience.wiley.com.]

a (100 mm Hg ≈ 13.3 kPa) pressure cuff on the forearm of PWS patients; the blood volume fraction was estimated to increase by a factor of 3 and vessel diameters by 1.7, and 40% lower fluence (585 nm, 0.45 milliseconds pulse) was needed to reach the same degree of purpura in the absence of the pressure. Figure 4a, b shows that higher blood and vessel temperatures are reached by increasing the diameter two fold from 10 μm to 20 μm. This change in diameter affects significantly the time-evolution of temperature during heating and cooling of the vessel, as seen in Figure 3a and b. Assuming that two- and threefold increases in vessel diameter are plausible, Figure 5 shows that small vessels (d<20 μm) would benefit from dilation if the final diameter is $\leq$30 μm, while medium and large diameters vessels would not.

Comparisons of temperature profiles for two different pressure conditions are shown in Figure 6. Although modeling at vacuum pressures includes a reduction in epidermal thickness and vertical vessel displacement and vessel dilation, the dominant effect in the temperature field is that more light is delivered to the blood and less energy is absorbed in the epidermis. The reduction in temperature across the epidermis is approximately 5°C in skin phototype II. For the 10 μm diameter vessel, the gain in temperature at the vessel center is greater than 10°C, Figure 6a. For the 60 μm diameter vessel, the maximum increase in temperature is ≈8°C at the top of the vessel, ≈3°C at the center, and ≈6°C at the bottom, Figure 6b. Note that the temperature at the vessel center still increases after laser irradiation. Figure 2b shows that modeling with the diffusion approximation results in more energy being absorbed near the vessel periphery (within the upper and lower half of the vessel) than at the center. After laser irradiation, heat diffusion from the vessel periphery increases the temperature at the vessel center. If the Monte Carlo method is used, more energy is absorbed within the upper part of the vessel and, consequently, the temperature at the vessel center would also increase after laser irradiation. Maxima in blood temperatures are secondary to our analysis since the objective is to increase the vessel wall temperature, which reaches peak values at the end of laser irradiation. Differences in temperature at the top of the vessel interior-wall between atmospheric and vacuum conditions are shown in Figure 7b as a function

of vessel diameter and depth. Clinical studies indicate that small vessel diameters of 10–20 μm at 250 μm depth persist after PDL multiple treatments [7,9]. Under 50 kPa vacuum pressure, these vessels would gain approximately an extra 10°C in wall temperature which might render the vessels more susceptible to irreversible thermal damage. Certainly, every vessel would gain more energy but the effect is more relevant in small vessels, which are currently extremely difficult to remove by PDL therapy. As vessel depth increases, the gain in temperature becomes similar for every vessel.

Figure 6a also shows that for higher melanin concentrations, reductions in epidermal temperature are significant (more than 10°C at the surface) and higher temperatures are reached within the vessel ($\Delta T_b^c \approx 10°C$, $\Delta T_w^t \approx 5°C$); however, melanin absorption is still considerable, which makes it difficult to treat safely PWS in patients with darker skin phototypes. The difference in temperature gradients at the epidermis between different skin phototypes is merely due to an instantaneous energy balance between a hot epidermis and cool dermis.

To model the effects of vacuum pressure on vessel diameter, we used a conservative 10% increase in dilation because our mechanical model predicts moderate changes in diameter; however, measurements using VRS show that larger vessel dilations are feasible [23]. It should be noted that reflectance spectra contain extensive information on skin morphology and optical structure, and that a challenging ill-posed mathematical problem must be solved to extract this data [25]. Currently, it is difficult to state with any degree of accuracy the weighted contribution of each specific effect—discussed in Section "Effects of Vacuum Pressure"—to changes in VRS measurements. Nevertheless, we also modeled vacuum pressure effects using dilations from VRS measurements. Figure 8 shows the combined effect of more light delivered to a larger blood volume on the temperature profile of a 10 μm diameter vessel under different vacuum pressures: at 17 kPa (5 in Hg), changes in epidermal absorption and thickness with respect to atmospheric pressure are small compared to changes in vessel diameter; at 34 kPa (10 in Hg), a further reduction in epidermal absorption and thickness continues while vessel diameter minimally increases; at 51 kPa (15 in Hg), epidermal absorption and thickness are further reduced and vessel diameter slightly increases. As expected, temperature gains in the blood vessel are even more significant, $\Delta T_c^b > 30°C$ and $\Delta T_w^t \approx 20°C$, while temperature reductions in the epidermis are similar to those obtained using our mechanical model.

CONCLUSIONS

Application of local vacuum pressure to PWS skin during laser irradiation results in less energy absorbed in the epidermis and more light delivered to an increased blood volume. Therefore, more energy deposition in a larger blood volume permits higher temperatures to be induced in vessel walls. Even though more energy is deposited in every vessel, temperature increases in vessels of 10–30 μm diameters are greater, increasing the likelihood of irreversible thermal damage to small resilient vessels. In addition, temperatures at the epidermis decrease because less energy is absorbed therein after local application of vacuum pressure.

ACKNOWLEDGMENTS

This work was supported by the following grants: AR47551, AR48458 and GM62177 to JSN and HD42057 to GA from the National Institutes of Health, and A. Ward Ford Grant to GA. Presentation of part of this work at the 2006 Annual Meeting of the American Society for Laser Medicine and Surgery was supported by a travel grant from the United States Air Force Office of Scientific Research to WF. Support in Finite Element Analysis provided by Dr. Rong Zhang is greatly appreciated.

REFERENCES

1. Anderson RR, Parrish JA. Microvasculature can be selectively damaged using dye lasers: A basic theory and experimental evidence in human skin. Lasers Surg Med 1981;1(3):263–276.
2. Nelson JS, Milner TE, Anvari B, Tanenbaum BS, Kimel S, Svaasand LO, Jacques SL. Dynamic epidermal cooling during pulsed-laser treatment of port-wine stain—A new methodology with preliminary clinical evaluation. Arch Dermatol 1995;131(6):695–700.
3. Nelson JS, Milner TE, Anvari B, Tanenbaum BS, Svaasand LO, Kimel S. Dynamic epidermal cooling in conjunction with laser-induced photothermolysis of port wine stain blood vessels. Lasers Surg Med 1996;19(2):224–229.
4. Lanigan SW. Port-wine stains unresponsive to pulsed dye laser: Explanations and solutions. Br J Dermatol 1998; 139(2):173–177.
5. Lanigan SW, Taibjee SM. Recent advances in laser treatment of port-wine stains. Br J Dermatol 2004;151(3):527–533.
6. Smit JM, Bauland CG, Wijnberg DS, Spauwen PHM. Pulsed dye laser treatment, a review of indications and outcome based on published trials. Br J Plast Surg 2005;58(7):981–987.
7. Fiskerstrand EJ, Dalaker M, Norvang LT. Laser treatment of port wine stains: A study comparing therapeutic outcome with morphologic characteristics of the lesions. Preliminary results. Acta Derm Venereol 1995;75(1):92–93.
8. Sivarajan V, Mackay IR. The depth measuring videomicroscope (dmv): A non-invasive tool for the assessment of capillary vascular malformations. Lasers Surg Med 2004; 34(2):193–197.
9. Sivarajan V, Mackay IR. Noninvasive in vivo assessment of vessel characteristics in capillary vascular malformations exposed to five pulsed dye laser treatments. Plast Reconstr Surg 2005;115(5):1245–1252.
10. Babilas P, Shafirstein G, Baumler W, Baier J, Landthaler M, Szeimies RM, Abels C. Selective photothermolysis of blood vessels following flashlamp-pumped pulsed dye laser irradiation: In vivo results and mathematical modelling are in agreement. J Invest Dermatol 2005;125(2):343–352.
11. Barsky SH, Rosen S, Geer DE, Noe JM. Nature and evolution of port wine stains: Computer assisted-study. J Invest Dermatol 1980;74(3):154–157.
12. Svaasand LO, Fiskerstrand EJ, Kopstad G, Norvang LT, Svaasand EK, Nelson JS, Berns MW. Therapeutic response during pulsed laser treatment of port-wine stains: dependence on vessel diameter and depth in dermis. Lasers Med Sci 1995;10(4):235–243.
13. Lucassen GW, Svaasand LO, Verkruysse W, VanGemert MJC. Original articles-laser energy threshold for thermal

vascular injury in a port-wine stain skin model. Lasers Med Sci 1995;10(4):231–234.
14. DeBoer JF, Lucassen GW, Verkruysse W, VanGemert MJC. Thermolysis of portwine-stain blood vessels: Diameter of a damaged blood vessel depends on the laser pulse length. Lasers Med Sci 1996;11(3):177–180.
15. Svaasand LO, Aguilar G, Viator JA, Randeberg LL, Kimel S, Nelson JS. Increase of dermal blood volume fraction reduces the threshold for laser-induced purpura: Implications for port wine stain laser treatment. Lasers Surg Med 2004;34(2):182–188.
16. Aguilar G, Svaasand LO, Nelson JS. Effects of hypobaric pressure on human skin: Feasibility study for port wine stain laser therapy (part I). Lasers Surg Med 2005;36(2):124–129.
17. Star W. Diffusion theory of light transport. In: Welch AJ, van Gemert MJC, editors. Optical-Thermal Response of Laser-Irradiated Tissue, New York: Plenum Press; 1995. pp. 131–206.
18. Jacques SL, Glickman RD, Schwartz JA. Internal absorption coefficient and threshold for pulsed laser disruption of melanosomes isolated from retinal pigment epithelium. In Proc. SPIE; 1996. volume 2681, 468–477.
19. Holman JP. Heat Transfer. New York: McGraw Hill; 1981.
20. van Gemert MJC, Welch AJ, Pickering JW, Oon TT. Laser treatment of port wine stains. In: Welch AJ, van Gemert MJC, editors. Optical-Thermal Response of Laser-Irradiated Tissue. New York: Plenum Publishing Corporation; 1995. 789–829.
21. Shafirstein G, Baumler W, Lapidoth M, Ferguson S, North P E, Waner M. A new mathematical approach to the diffusion approximation theory for selective photothermolysis modeling and its implication in laser treatment of port-wine stains. Lasers Surg Med 2004;34(4):335–347.
22. Chato JC. Selected thermophysical properties of biological materials. In: Shitzer A, Eberhart RC, editors. Heat Transfer in Medicine and Biology: Analysis and Applications, New York: Plenum Press; 1985. volume 2:413.
23. Childers M, Franco W, Nelson JS, Aguilar G. Laser surgery of port wine stains using local vacuum pressure: changes in skin morphology and optical properties (part I). Lasers Surg Med 2007;39(2):108–117.
24. Pfefer JT, Barton JK, Chan EK, Ducros MG, Sorg B, Milner TE, Nelson JS, Welch AJ. A three-dimensional modular adaptable grid numerical model for light propagation during laser irradiation of skin tissue. IEEE J Sel Top Quantum Electr 1996;2(4):934–942.
25. Verkruysse W, Zhang R, Choi B, Lucassen G, Svaasand LO, Nelson JS. A library based fitting method for visual reflectance spectroscopy of human skin. Phys Med Biol 2005;50:57–70.